Configurational anisotropic spin waves in cross-shaped $Ni_{80}Fe_{20}$ nanoelements

B. K. Mahato, B. Rana, R. Mandal, D. Kumar, S. Barman, Y. Fukuma, Y. Otani, and A. Barman

Citation: Appl. Phys. Lett. **102**, 192402 (2013);
View online: https://doi.org/10.1063/1.4804990
View Table of Contents: http://aip.scitation.org/toc/apl/102/19
Published by the American Institute of Physics

Configurational anisotropic spin waves in cross-shaped $Ni_{80}Fe_{20}$ nanoelements

B. K. Mahato,[1] B. Rana,[1] R. Mandal,[1] D. Kumar,[1] S. Barman,[1] Y. Fukuma,[2,3] Y. Otani,[2,4] and A. Barman[1,a)]

[1]*Thematic Unit of Excellence on Nanodevice Technology and Department of Condensed Matter Physics and Material Sciences, S. N. Bose National Centre for Basic Sciences, Block JD, Sector III, Salt Lake, Kolkata 700 098, India*
[2]*Advanced Science Institute, RIKEN, 2-1 Hirosawa, Wako, Saitama 351-0198, Japan*
[3]*Frontier Research Academy for Young Researchers, Kyushu Institute of Technology, lizuka, Fukuoka 820-8502, Japan*
[4]*Institute for Solid State Physics, University of Tokyo, 5-1-5 Kashiwanoha, Kashiwa, Chiba 277-8581, Japan*

(Received 8 March 2013; accepted 27 April 2013; published online 13 May 2013)

Optically induced spin waves in $Ni_{80}Fe_{20}$ (permalloy) cross-shaped nanoelements are studied by time-resolved magneto-optical Kerr effect microscope. A strong anisotropy in the spin wave modes are observed with the orientation angle (ϕ) of the in-plane bias magnetic field. As ϕ deviates from 0° a single resonant mode splits into a numbers of modes, while the powers of the higher frequency modes increase as ϕ increases from 0 to 45°. The lowest frequency mode shows a four-fold configurational anisotropy. The mode of a single cross remains unaffected by the magnetostatic interaction of the neighbouring elements for $\phi = 0°$, while the effect increases with ϕ and becomes maximum at 45°, making these elements interesting candidates as building blocks for magnonic devices. © *2013 AIP Publishing LLC*. [http://dx.doi.org/10.1063/1.4804990]

Current trend in the miniaturization of magnetoelectronic and data storage devices with faster response and lower energy consumption demands the study of the magnetization processes of magnetic nanostructures at very small time- and length-scales.[1–4] Emerging technologies such as spin torque nano-oscillators as on-chip microwave sources,[5] magnonic crystals as on-chip data communications,[6,7] and spin based logic devices[8,9] pose challenges towards manipulation of magnetization dynamics not only by varying the magnetic materials but also by varying the size, shape, and aspect ratio of a given material. In addition to the physical structures of the individual elements, the magnetic properties of the nanomagnetic metamaterials in the form of artificial lattices may also be tailored by varying the shapes of the individual elements. The magnetization of confined magnetic elements deviates from the bias magnetic field even in presence of a large enough magnetic field thus creating demagnetized regions. These demagnetized regions play important roles in determining their magnetic ground states as well as the magnetization dynamics. They offer different potentials to the propagating spin waves and also spatially localize them within the demagnetized regions. In addition, the inter-dot magnetostatic interaction[10–12] in ordered arrays of nanomagnets may also get affected by the shapes of the elements. This is because the profile of the stray magnetic field depends on the shapes of the boundaries of the elements as well as the internal magnetic field.

Recent developments in the fabrication of ordered arrays of nanostructures of various geometric shapes have opened the opportunity to study the shape dependent magnetic properties of nanomagnets and their potential applications.[13,14] Rotational symmetry of various orders based upon the symmetry of the nanomagnets has been reported from the measurements of in-plane magnetic hysteresis loops.[13–15] Control of configurational anisotropy through edge indentation of permalloy square prisms and thereby affecting their micromagnetic configurations has been demonstrated.[16] Four-fold anisotropy in the precession frequency and damping in square magnetic microelement due to the systematic variation of the inhomogeneous internal field of the elements with the orientation of the bias magnetic field were investigated by time-resolved Kerr microscopy.[17] Later, dynamical configurational anisotropy of various symmetry were observed in arrays of nanoelements[18–20] originating not only from the internal magnetic fields of the elements but also from the symmetry of the magnetostatic stray field within an array of nanoelements showing collective magnetization dynamics. Brillouin light scattering experiments on triangular[21] and elliptical dots with "egg-like" distortion[22] showed localized modes and mode distortion affecting the linewidth of the mode spectra. Three dimensional shape dependent spin wave modes were also demonstrated recently.[23]

Static magnetic spin configurations in permalloy cross-shaped structure studied by magnetic force microscope showed magnetic poles and complex spin configurations at the junction of the cross.[24] However, spin wave modes in such structures have not been reported. Here, we present the anisotropy in the spin wave mode in a cross-shaped permalloy element by an all-optical time-resolved magneto-optical Kerr effect (TRMOKE) microscope. We have used micromagnetic simulations to understand the frequency spectra and the spatial profiles of the modes.

Arrays of cross-shaped permalloy elements with total length and width of about 600 nm, thickness of 20 nm, and nearest edge spacing of 50 nm were fabricated by e-beam lithography and e-beam evaporation. The scanning electron

a)abarman@bose.res.in

micrograph (Fig. 1(a)) showed that the cross-shapes have slightly rounded corners. The time-resolved magnetization dynamics of a permalloy film of 20 nm thickness deposited under the same condition was measured by an all-optical TRMOKE microscope[25] for extraction of the materials parameters. The frequency of uniform precession is plotted as a function of the bias field (Fig. 1(b)) and was fitted with Kittel's formula. The time-resolved magnetization dynamics from the cross-shaped element is measured with a collinear pump-probe arrangement. The focused probe beam ($\lambda = 800$ nm) with about 700 nm spot size probes the dynamics of a single element under the influence of the magnetostatic interaction from the neighbouring elements. The pump beam has central wavelength of $\lambda = 400$ nm and has a spot size of about 1 μm. The pump and probe spots are schematically shown on the SEM image in Fig. 1(a). The pump and probe fluences used in this experiment are about 12 mJ/cm^2 and 2 mJ/cm^2, respectively. The applied bias magnetic field is tilted at a small angle to the plane of the elements, while the in-plane component of that field is denoted by H in Fig. 1(a). The time-resolved data was measured as a function of the azimuthal angle ϕ for $H = 0.87$ kOe. The value of $H = 0.87$ kOe is found to be the maximum bias field, which remained stable during the measurements of time-resolved magnetization dynamics at varying ϕ between 0 and 180° in our measurement. Micromagnetic simulations of the static magnetic configurations of the elements using OOMMF software[26] showed that at $H = 0.87$ kOe the elements have similar magnetization distribution to that for $H >$ saturation fields as obtained from the simulated hysteresis loops.

The precessional dynamics appears as an oscillatory signal above a slowly decaying part of the time-resolved Kerr rotation data followed by demagnetization within 400 fs and a fast remagnetization within 10 ps. A bi-exponential background was subtracted from the time-resolved data, and fast Fourier transform (FFT) was performed to find out the frequency spectra.[25] Figures 1(c) and 1(d) show the experimental time-resolved Kerr rotations at different values of ϕ and the corresponding FFT spectra. At $\phi = 0°$, a single dominant mode is observed at about 5.5 GHz, but as ϕ is deviated from 0° a number of modes appear. At $\phi = 15°$, four clear modes appear, while for $\phi = 30$ and 45° five modes with significant intensities appear. For $\phi = 45°$ the intensities of the additional peaks reach a maximum. As ϕ is further increased the trend is repeated and at $\phi = 90°$ again a single dominant mode similar to $\phi = 0°$ is observed. The lowest frequency mode shows a four-fold anisotropy as a function of ϕ as shown in Fig. 2(a).

Micromagnetic simulations of the spin wave spectra were performed by OOMMF. The shapes of the elements were derived from the SEM images and were discretized into rectangular prism like cells of $4 \times 4 \times 20$ nm^3 dimensions. Further test simulations with smaller cell sizes along the lateral directions and along the thickness showed that spin wave modes remain qualitatively similar. The material parameters were used as $\gamma = 18.5$ MHz/Oe, $H_K = 0$, $M_S = 860$ emu/cc as extracted from the Kittel's fit to the precession frequency vs. bias field described before, while the exchange stiffness constant is used as $A = 1.3 \times 10^{-6}$ erg/cm.[27] The optical excitation is approximated by a pulsed magnetic

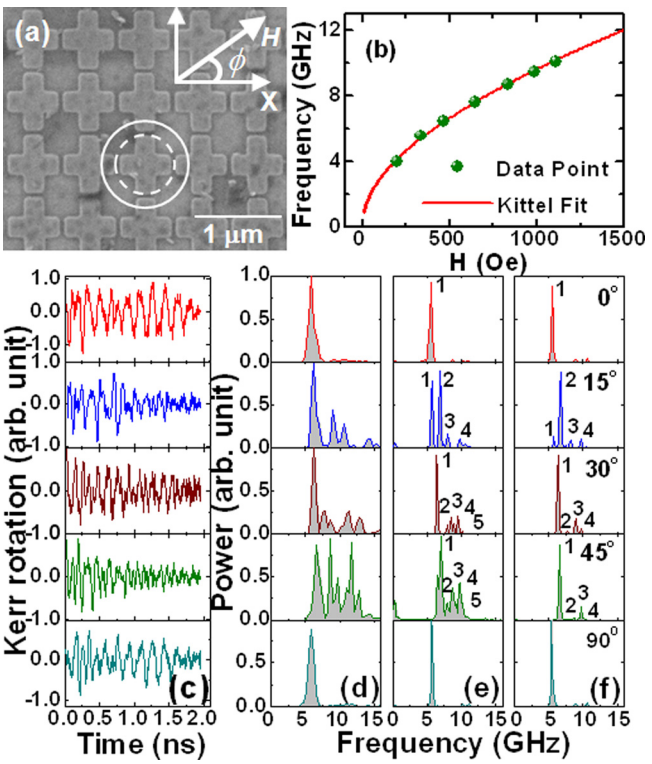

FIG. 1. (a) Scanning electron micrograph of the array of cross-shaped permalloy elements. The solid and dotted circles represent the schematic of the pump and probe spots on the sample. The geometry of the bias magnetic field is shown on the SEM image. (b) Frequency vs. bias magnetic field for a permalloy thin film with 20 nm thickness along with the fit with Kittel's formula. (c) Measured time-resolved Kerr rotation and (d) the corresponding FFT spectra from the array of cross-shaped permalloy elements at different orientations of the bias magnetic field ϕ. Simulated spin wave spectra from (e) a 3×3 array of cross-shaped elements and (f) a single cross-shaped element at same values of ϕ.

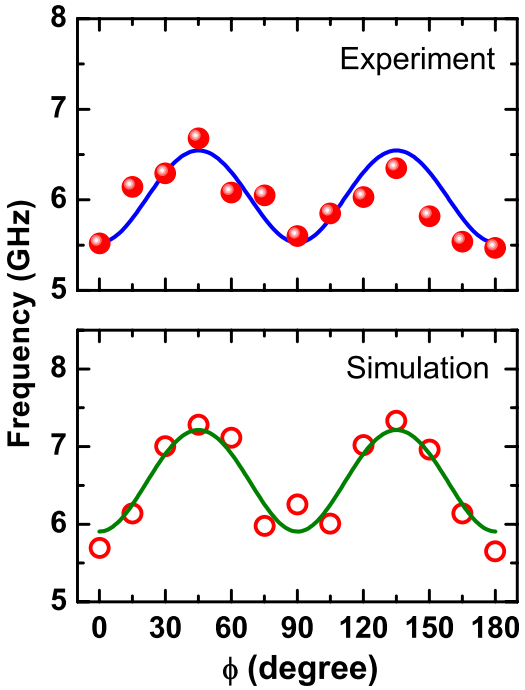

FIG. 2. Experimental and simulated frequencies as a function of the azimuthal angle ϕ of the bias magnetic field. The solid lines show a fit to a solution of LLG equation with a four-fold anisotropy.

field with risetime of 50 ps and peak value of 30 Oe, applied along the normal to the sample plane. The FFT spectra of the simulated time-dependent magnetization of a 3×3 array of cross-shaped elements are shown in Fig. 1(e). The simulated spectra shows similar features as the experimental data such as a single resonant mode for $\phi = 0$ and 90° while a band of modes are observed for 15, 30, and 45°. The lowest frequency mode in the simulated spectra also shows a four-fold variation as a function of ϕ as shown in Fig. 2(b). The variation of precession frequency with ϕ has been modelled by solving Landau-Lifshitiz-Gilbert equation with a four-fold anisotropy field,[17] and the anisotropy field is found to be about 35 Oe and 40 Oe in the experiment and the simulation, respectively. The deviation in the simulated anisotropy field from the experimental value is possibly due to the limitation in the reproduction of the shapes and defects present in the experimental sample due to the relatively large value of the cell size compared to the rounded features of the cross-shaped samples.

In order to understand the effect of the magnetostatic interaction between the neighbouring elements, we have simulated the spin wave spectra for a single cross-shaped element (Fig. 1(f)) under similar conditions as for the array. A comparison shows that while for $\phi = 0°$ the two spectra are identical, differences arise as ϕ deviates from 0°, and becomes maximum for $\phi = 45°$. The intensities of the higher frequency peaks are higher for the array as compared to the single element, and an additional peak becomes prominent for $\phi = 30$ and 45°, showing the stronger effect of the magnetostatic interactions. We have further calculated the spatial distributions of powers and phases of the individual resonant modes observed in the spectra by using a home built code.[28] Figures 3 and 4 show the power profiles of all resonant modes for the 3×3 array and the single element, respectively. The colormap is shown next to the mode profiles. The single resonant mode for $\phi = 0°$ shows an "X" like pattern extended in the vertical arms of the cross with its centre at the centre of the cross. This mode also has some power at the ends of the horizontal arm. This mode profile is identical to that observed for a single cross. As ϕ deviates from 0°, the modes starts to flow more into the horizontal arms of the cross, and a number of quantized modes are now accommodated within the cross with the quantization axis parallel to the direction of the bias field. The mode quantization number increases with the increase in mode frequency. These higher frequency modes get increasingly more power as ϕ varies from 0 to 45°. In addition, the mode profiles and the powers on these modes get increasingly more affected in the array as compared to the single element as ϕ varies from 0 to 45°. In Fig. 3(b), we show the mode profiles for $\phi = 0°$ calculated with two cell sizes of $4 \times 4 \times 4\,\text{nm}^3$ and $2 \times 2 \times 20\,\text{nm}^3$. Although the power distributions of the modes slightly differ with cell size, the modes remained qualitatively same with cell size.

For further understanding of the mode profiles and the effects of the neighbouring elements on the mode profiles, we have numerically calculated the magnetostatic field distribution as shown in Fig. 5. For $\phi = 0°$, the non-uniform magnetization within the elements is concentrated near the edges of the horizontal and the vertical arms of the cross

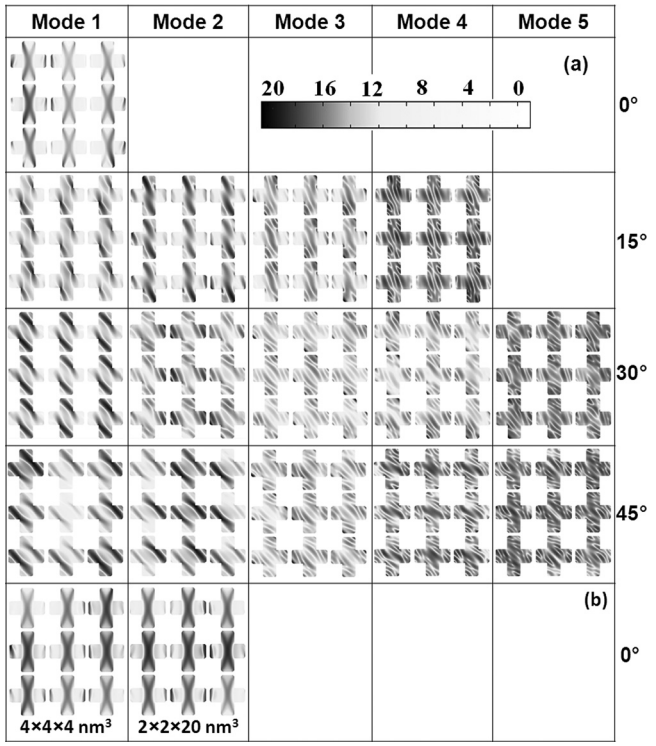

FIG. 3. (a) Simulated spatial distributions of power corresponding to different resonant modes, as shown in Figure 1(e) for a 3×3 array of cross-shaped permalloy elements with the bias field applied at different angles ϕ *w.r.t.* the array. (b) Test simulations with smaller cell sizes for $\phi = 0°$. The colorscale for power is shown at the top of the figure.

parallel to the bias field defining the regions where the modes are concentrated within the cross. The stray magnetic fields are also concentrated just outside those edges thereby limiting the stray fields to affect the modes of the individual elements significantly. As ϕ deviates from 0° the internal non-uniform magnetization regions also rotate creating an

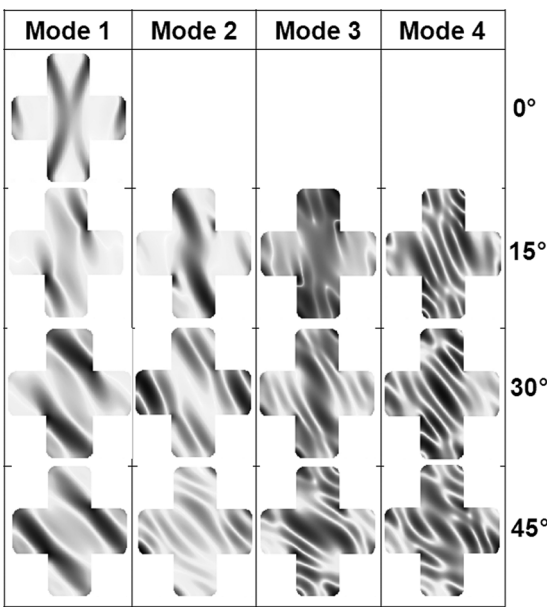

FIG. 4. Simulated spatial distributions of power corresponding to different resonant modes as shown in Figure 1(f) for a single cross-shaped permalloy element with the bias magnetic field applied at different angles ϕ *w.r.t.* the element. The colorscale for power is as shown in Figure 3.

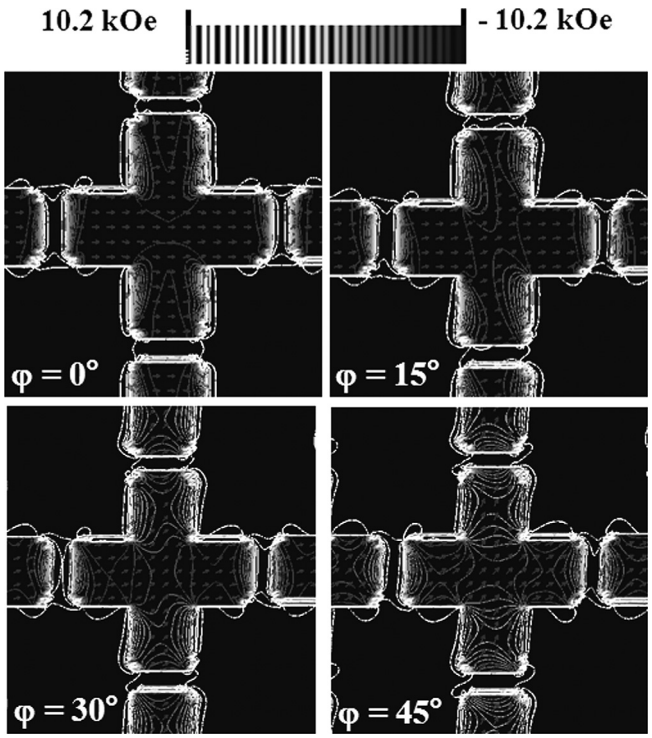

FIG. 5. Simulated magnetostatic field distributions inside and around the central element of a 3 × 3 array of cross-shaped elements with the bias magnetic field applied at different angles ϕ *w.r.t.* the array. The colorscale is shown at the top of the figure.

asymmetry and allowing the modes to leak into the horizontal arms. The quantized modes now form due to the corresponding physical boundaries and the resulting demagnetizing fields. The stray magnetic fields from the neighbouring elements start to extend increasingly more, reaching inside the elements and thereby affecting the modes to larger extent. This reaches a maximum for $\phi = 45°$ and decreases again following the symmetry of the element. The four-fold anisotropy for the lowest frequency mode is also originated due to the above variation of the magnetostatic field.

In summary, we have investigated optically excited spin wave modes in arrays of cross shaped permalloy elements of about 600 nm length and width, 20 nm thickness, and about 50 nm separation between the nearest edges. We have used a custom built two color all-optical TRMOKE microscope for this investigation under the application of a bias magnetic field, whose orientation ϕ is varied with respect to the sample geometry. A significant anisotropy in the nature and frequencies of the spin wave modes with ϕ is observed. When the bias field is applied parallel to one of the arms of the cross ($\phi = 0°$ and 90°) a dominant single mode is observed, while a band of modes appear as ϕ deviates from 0° and 90° and the band becomes broadest at $\phi = 45°$. The lowest frequency mode shows a four-fold anisotropy. Micromagnetic simulations qualitatively reproduce the experimentally observed features. The simulated mode profiles show the occurrence of a number of quantized modes, where the frequencies of the modes increase with the mode quantization numbers. The frequencies and profiles of the modes of the elements in the array are significantly affected by the neighboring elements as ϕ deviates from 0° and become maximum at 45°. The observed anisotropy in the spin wave modes and its collective behavior are significant for building future magnonic nanodevices based upon cross-shaped magnetic nanoelements.

The authors gratefully acknowledge the financial supports from the Department of Science and Technology, Government of India under Grant Nos. SR/NM/NS-53/2010, INT/EC/CMS (24/233552), INT/JP/JST/P-23/09, and SR/WOS-A/PS-27/2010, Department of Information Technology, Government of India under Grant No. 1(7)/2010/M&C, and Japan Science and Technology Agency Strategic International Cooperative Program under Grant No. 09158876. B.K.M. and D.K. acknowledge CSIR and B.R. acknowledges UGC, Government of India for senior research fellowships.

[1]R. Skomski, J. Phys.: Condens. Matter **15**, R841 (2003).
[2]B. D. Terris and T. Thomson, J. Phys. D: Appl. Phys. **38**, R199 (2005).
[3]A. Barman, S. Wang, J. D. Maas, A. R. Hawkins, S. Kwon, A. Liddle, J. Bokor, and H. Schmidt, Nano Lett. **6**, 2939 (2006).
[4]A. Laraoui, J. Vénuat, V. Halté, M. Albrecht, E. Beaurepaire, and J.-Y. Bigot, J. Appl. Phys. **101**, 09C105 (2007).
[5]S. Kaka, M. R. Pufall, W. H. Rippard, T. J. Silva, S. E. Russek, and J. A. Katine, Nature (London) **437**, 389 (2005).
[6]V. V. Kruglyak, S. O. Demokritov, and D. Grundler, J. Phys. D: Appl. Phys. **43**, 264001 (2010).
[7]B. Lenk, H. Ulrichs, F. Garbs, and M. Münzenberg, Phys. Rep. **507**, 107 (2011).
[8]D. A. Allwood, G. Xiong, C. C. Faulkner, D. Atkinson, D. Petit, and R. P. Cowburn, Science **309**, 1688 (2005).
[9]A. Khitun, M. Bao, and K. L. Wang, IEEE Trans. Magn. **44**, 2141 (2008).
[10]R. Zivieri, F. Montoncello, L. Giovannini, F. Nizzoli, S. Tacchi, M. Madami, G. Gubbiotti, G. Carlotti, and A. O. Adeyeye, Phys. Rev. B **83**, 054431 (2011).
[11]B. Rana, S. Pal, S. Barman, Y. Fukuma, Y. Otani, and A. Barman, Appl. Phys. Express **4**, 113003 (2011).
[12]Z. K. Wang, H. S. Lim, V. L. Zhang, J. L. Goh, S. C. Ng, M. H. Kuok, H. L. Su, and S. L. Tang, Nano Lett. **6**, 1083 (2006).
[13]A. O. Adeyeye and N. Singh, J. Phys. D: Appl. Phys. **41**, 153001 (2008).
[14]R. P. Cowburn, A. O. Adeyeye, and M. E. Welland, Phys. Rev. Lett. **81**, 5414 (1998).
[15]R. P. Cowburn, D. K. Koltsov, A. O. Adeyeye, and M. E. Welland, Europhys. Lett. **48**, 221 (1999).
[16]D. K. Koltsov and M. E. Welland, J. Appl. Phys. **94**, 3457 (2003).
[17]A. Barman, V. V. Kruglyak, R. J. Hicken, A. Kundrotaite, and M. Rahman, Appl. Phys. Lett. **82**, 3065 (2003).
[18]V. V. Kruglyak, P. S. Keatley, R. J. Hicken, J. R. Childress, and J. A. Katine, Phys. Rev. B **75**, 024407 (2007).
[19]B. Rana, D. Kumar, S. Barman, S. Pal, R. Mandal, Y. Fukuma, Y. Otani, S. Sugimoto, and A. Barman, J. Appl. Phys. **111**, 07D503 (2012).
[20]S. Saha, R. Mandal, S. Barman, D. Kumar, B. Rana, Y. Fukuma, S. Sugimoto, Y. Otani, and A. Barman, "Tunable Magnonic Spectra in Two-Dimensional Magnonic Crystals with Variable Lattice Symmetry," Adv. Funct. Mater (to be published).
[21]C. S. Lin, H. S. Lim, C. C. Wang, A. O. Adeyeye, Z. K. Wang, S. C. Ng, and M. H. Kuok, J. Appl. Phys. **108**, 114305 (2010).
[22]H. T. Nembach, J. M. Shaw, T. J. Silva, W. L. Johnson, S. A. Kim, R. D. McMichael, and P. Kabos, Phys. Rev. B **83**, 094427 (2011).
[23]R. Brandt, F. Ganss, R. Rückriem, T. Senn, C. Brombacher, P. Krone, M. Albrecht, and H. Schmidt, Phys. Rev. B **86**, 094426 (2012).
[24]K. Machidaa, T. Tezuka, T. Yamamoto, T. Ishibashi, Y. Morishita, A. Koukitu, and K. Sato, J. Magn. Magn. Mater. **290–291**, 779 (2005).
[25]B. Rana, D. Kumar, S. Barman, S. Pal, Y. Fukuma, Y. Otani, and A. Barman, ACS Nano **5**, 9559 (2011).
[26]M. J. Donahue and D. G. Porter, OOMMF User's Guide, version 1.0, National Institute of Standard and Technology, Gaithersburg, MD, 1999, Interagency Report NISTIR 6376. See http://math.nist.gov/oommf.
[27]K. H. J. Buschow, *Handbook of Magnetic Materials* (Amsterdam, North Holland, The Netherlands, 2009), Vol. 18, p. 168.
[28]D. Kumar, O. Dmytriiev, S. Ponraj, and A. Barman, J. Phys. D: Appl. Phys. **45**, 015001 (2012).